

Modelling flow-distributed oscillations in the CDIMA reaction

Jonathan R. Bamforth,^{ab} Serafim Kalliadasis,^b John H. Merkin^c and Stephen K. Scott^a

^a School of Chemistry, University of Leeds, Leeds, UK LS2 9JT

^b Department of Chemical Engineering, University of Leeds, Leeds, UK LS2 9JT

^c Department of Applied Mathematics, University of Leeds, Leeds, UK LS2 9JT

Received 7th June 2000, Accepted 24th July 2000

Published on the Web 4th September 2000

The development of spatial patterns ('flow distributed oscillations') in a model representing the chlorine dioxide–iodine–malonic acid (CDIMA) reaction is investigated analytically and numerically. Flow distributed oscillations arise in a plug-flow reactor (PFR) for which the inflow concentrations of the various reacting species are maintained at appropriate constant values. Unlike other situations, the patterning here does not require any difference in diffusion coefficients for the different species. The patterns are, however, closely related to operating conditions for which the same chemical system would show temporal oscillations in a well-stirred batch reactor. As the flow rate through the PFR is varied, the system undergoes a sequence of transitions from absolute to convective instability and subsequently to stationary patterns. The onset of stationary patterns is found to be subcritical, so there is a range of operating conditions for which there is bistability between a stationary pattern and an essentially uniform state. The results indicate that these patterns occur for conditions that should be realisable experimentally and that typical wavelengths of the patterns would be of the order of 0.1 mm.

1. Introduction

The spontaneous formation of spatial structure (non-uniform concentration distributions) in reacting chemical systems exhibiting feedback kinetics is an active area of current research.^{1,2} The most well-known mechanism for the generation of such structure is, perhaps, the 'diffusion-driven' or Turing instability³ through which the uniform steady state becomes unstable to spatial perturbation of some appropriate wavelength. This mechanism relies on selected species (generally the feedback species) having a reduced mass diffusivity compared to other reacting species. In the 'differential flow induced chemical instability' (DIFICI), spatial patterns may develop if any one of the important reacting species has a reduced diffusivity.^{4,5} Differential diffusion or flow is not, however, a necessary requirement for pattern formation. The Couette reactor, for instance, supports patterns under conditions for which all species have essentially the same mass transport characteristics^{6–11} (typically represented by an enhanced diffusion coefficient¹²).

Very recently, Kuznetsov *et al.* have proposed¹³ a pattern-formation mechanism which also operates with equal diffusivities. The experimental configuration envisaged is simply that of a reactor along which the reacting mixture is flowed at some constant velocity. The concentrations at the inflow are maintained at some fixed value but then may vary in space (and time) along the reactor. Such 'plug flow reactors' are of widespread use in industry. The kinetic parameters within the reactor for the conditions of interest are such that the same reaction in a well-stirred batch reactor would show a spontaneous oscillatory response. The spatial patterns that arise in the plug-flow reactor have been termed 'flow distributed oscillations' (FDO). Kuznetsov *et al.* and Andresen *et al.* determined the conditions^{13,14} for such pattern formation through analysis and computation based on the classic Brusselator model for chemical oscillations. Kaern and Menzinger demonstrated this phenomenon experimentally,¹⁵ exploiting

the Belousov–Zhabotinsky (BZ) reaction and using the outflow from a well-stirred flow reactor operating under steady state conditions to provide the input to the plug flow reactor. The BZ reaction is an excitable system with two distinct time scales for the evolution of the relevant species concentration, and thus is typically somewhat different in character from Brusselator-type systems, but this work clearly established this effect as a real feature.

In the present paper, we study the conditions for FDO in a model of a real chemical reaction which exhibits oscillatory behaviour more characteristic of Brusselator-type instabilities, *i.e.* the chlorine dioxide–iodine–malonic acid (CDIMA) reaction¹⁶ (which is also the system for which experimental examples of Turing patterns have been obtained^{17,18}). We show that FDO patterns are predicted over a range of experimental conditions for this reaction, with other spatiotemporal behaviour predicted outside these conditions. Despite the expected qualitative similarities of the response of the CDIMA and Brusselator systems, we observe a significant difference close to the onset of FDO.

The model and governing equations are presented and reduced to an appropriate dimensionless form in section 2. The resulting equations are analysed on an infinite spatial domain in section 3, which provides the main results for the predicted instability loci. We address the stability of the inflow or boundary conditions in section 4, and then present our computational results in section 5.

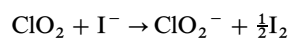
2. Model and governing equations

The experimental configuration comprises an essentially 1-D plug-flow reactor (PFR) along which the reacting mixture flows with a uniform velocity ϕ_p . The inflow to the reactor is provided by the outflow from a continuous-flow, well-stirred tank reactor (CSTR) through which the solution has a flow rate ϕ_c . We assume that the reaction follows the Lengyel–Epstein model^{19,20} for the CDIMA reaction. In this reaction,

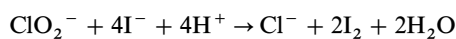
the reactor is supplied with reactants malonic acid (MA), chlorine dioxide (ClO₂) and iodine (I₂). The important intermediate species concentration are iodide I⁻ and chlorite ClO₂⁻ ions, and these participate in the following three component stoichiometric processes:



$$r_1 = \frac{k_{1\alpha}[\text{MA}][\text{I}_2]}{k_{1\beta} + [\text{I}_2]} \quad (1)$$



$$r_2 = k_2[\text{ClO}_2][\text{I}^-] \quad (2)$$



$$r_3 = \frac{k_{3\beta}[\text{ClO}_2^-][\text{I}_2][\text{I}^-]}{k_{3\gamma} + [\text{I}^-]^2} \quad (3)$$

The concentrations of the ‘pool chemical’ reactants MA, ClO₂ and I₂ will be taken as imposed constants or parameters and the products IMA and Cl⁻ will not be considered explicitly.

For the PFR, the governing mass-balance equations can be written in the form:

$$\frac{\partial \bar{u}}{\partial \bar{t}} + \bar{\phi}_p \frac{\partial \bar{u}}{\partial \bar{x}} = \bar{D}_u \frac{\partial^2 \bar{u}}{\partial \bar{x}^2} + r_1 - r_2 - 4r_3 \quad (4a)$$

$$\frac{\partial \bar{v}}{\partial \bar{t}} + \bar{\phi}_p \frac{\partial \bar{v}}{\partial \bar{x}} = \bar{D}_v \frac{\partial^2 \bar{v}}{\partial \bar{x}^2} + r_2 - r_3 \quad (4b)$$

where \bar{u} and \bar{v} are the concentration of I⁻ and ClO₂⁻ respectively and $\bar{D}_{u,v}$ represent the diffusion coefficients for these species (see list of symbols in Table 1). These equations can be

written in the following dimensionless form:

$$\frac{\partial u}{\partial t} + \phi_p \frac{\partial u}{\partial x} = \frac{\partial^2 u}{\partial x^2} + 1 - u - \frac{4uv}{\beta + u^2} \quad (5a)$$

$$\frac{\partial v}{\partial t} + \phi_p \frac{\partial v}{\partial x} = \sigma \frac{\partial^2 v}{\partial x^2} + \alpha \left(u - \frac{uv}{\beta + u^2} \right) \quad (5b)$$

(see list of symbols in Table 2). This scaling is consistent with that introduced in our previous paper¹² but differs slightly from that adopted by Lengyel and Epstein.^{19,20} The parameter σ is the ratio of the diffusion coefficients for the two species. To exclude specifically any possibility of spatial instabilities arising through the Turing mechanism, we will take $\sigma = 1$ throughout this work. The parameter α is effectively a scaled ratio of the inflow concentration of I₂ to that of MA and, along with the dimensionless flow velocity ϕ_p , will be treated as an experimental control (or bifurcation) parameter. The parameter β will be treated as a small fixed constant with $\beta = 10^{-4}$ throughout.

Eqn. (5) holds over a reactor of dimensionless length L and is subject to imposed boundary conditions at $x = 0$ and $x = L$. The ‘inflow’ boundary conditions at $x = 0$ are set by the concentrations of the intermediate species in the CSTR. These are governed by the following mass-balance equations:

$$\frac{du_C}{dt} = 1 - u_C - \frac{4u_C v_C}{\beta + u_C^2} - \phi_C u_C \quad (6a)$$

$$\frac{dv_C}{dt} = \alpha \left(u_C - \frac{u_C v_C}{\beta + u_C^2} \right) - \phi_C v_C \quad (6b)$$

We assume that these impose the values of the variables at $x = 0$, namely

$$u = u_C, \quad v = v_C \quad \text{at} \quad x = 0 \quad (7)$$

Table 1 List of symbols used for physical parameters

Symbol	Meaning	Units
$\bar{D}_{u,v}$	diffusion coefficient of I ⁻ and ClO ₂ ⁻	m ² s ⁻¹
\bar{l}_{ref}	$= \sqrt{\bar{D} \bar{t}_{\text{ref}}}$, reference length scale	m
\bar{t}	time	s
\bar{t}_{ref}	$= \frac{1}{k_2[\text{ClO}_2]_0}$, reference time scale	s
\bar{u}, \bar{v}	concentration of I ⁻ , ClO ₂ ⁻	mol dm ⁻³
\bar{x}	distance	m
$\bar{\phi}_C$	inverse residence time in CSTR	s ⁻¹
$\bar{\phi}_p$	flow velocity in PFR	m s ⁻¹
U_s	$= \frac{k_{1\alpha}[\text{MA}][\text{I}_2]}{k_2[\text{ClO}_2](k_{1\beta} + [\text{I}_2])}$, reference concentration for I ⁻	mol dm ⁻³
V_s	$= \frac{(k_{1\alpha}[\text{MA}])^2[\text{I}_2]}{k_{3\beta} k_2[\text{ClO}_2](k_{1\beta} + [\text{I}_2])^2}$, reference concentration for ClO ₂ ⁻	mol dm ⁻³

Table 2 List of symbols used for dimensionless parameters

Symbol	Definition	Meaning
$\bar{D}_{u,v}$	$\frac{\bar{D}_{u,v}}{k_2[\text{ClO}_2]_{\text{ref}} \bar{l}_{\text{ref}}^2}$	dimensionless diffusion coefficients
t	$\frac{\bar{t}}{\bar{t}_{\text{ref}}}$	dimensionless time
u	$\frac{\bar{u}}{U_s}$	dimensionless concentration of I ⁻
v	$\frac{\bar{v}}{V_s}$	dimensionless concentration of ClO ₂ ⁻
x	$\frac{\bar{x}}{\bar{l}_{\text{ref}}}$	dimensionless distance
α	$\frac{U_s}{V_s}$	dimensionless kinetic parameter
β	$\frac{k_{3\gamma}}{U_s^2}$	dimensionless kinetic parameter
ϕ_C	$\frac{\bar{\phi}_C}{k_2[\text{ClO}_2]}$	dimensionless inverse residence time for CSTR
ϕ_p	$\frac{\bar{\phi}_p}{k_2[\text{ClO}_2]_{\text{ref}} \bar{l}_{\text{ref}}}$	dimensionless flow velocity in PFR
κ		dimensionless wavenumber
λ	$1/\kappa$	dimensionless wavelength
ω_0		dimensionless oscillatory period of batch reactor system

for the PFR. Eqn. (6) admits a single physically acceptable steady state solution ($u_{\text{Css}}, v_{\text{Css}}$) satisfying $du_C/dt = dv_C/dt = 0$ in the CSTR, and if this steady state is stable (see section 4) we can impose

$$u = u_{\text{Css}}, \quad v = v_{\text{Css}} \quad \text{at} \quad x = 0 \quad (8)$$

At the outflow of the PFR, we adopt zero-flux boundary conditions so there is no mass transfer back into the PFR

$$\partial u/\partial x = \partial v/\partial x = 0 \quad \text{at} \quad x = L. \quad (9)$$

We shall assume that the dimensionless length of the reactor L is large and, for the theoretical analysis in the next section, we shall assume the boundary condition (9) applies as $x \rightarrow \infty$.

3. Linear stability analysis for PFR

We begin our analysis by determining the spatially uniform steady-states of eqn. (5). The system possesses a single steady state (u_s, v_s) satisfying

$$1 - u_s - \frac{4u_s v_s}{\beta + u_s^2} = u_s - \frac{u_s v_s}{\beta + u_s^2} = 0 \quad (10a)$$

giving

$$u_s = \frac{1}{5}, \quad v_s = \frac{1}{25} + \beta \quad (10b)$$

A straightforward local stability analysis of the reaction rate equations for a corresponding well-stirred batch system with the same kinetics reveals a Hopf bifurcation at $\alpha = \alpha_H$ with

$$\alpha_H = \frac{3}{5} - 25\beta \quad (11)$$

The uniform steady state for the batch system is then stable for $\alpha > \alpha_H$. It is also important here to note that the Hopf bifurcation for this system is subcritical for $\beta < 2.9 \times 10^{-3}$ and supercritical for larger values of β . In the present paper, we will typically take $\beta = 10^{-4}$, so the bifurcation is subcritical in this case.

The stability of the PFR can be determined by introducing a small perturbation (U, V) of the form $u = u_s + U, v = v_s + V$, leading to the linearised equations

$$\frac{\partial U}{\partial t} + \phi_P \frac{\partial U}{\partial x} = \frac{\partial^2 U}{\partial x^2} + j_{11}U + j_{12}V \quad (12a)$$

$$\frac{\partial V}{\partial t} + \phi_P \frac{\partial V}{\partial x} = \frac{\partial^2 V}{\partial x^2} + j_{21}U + j_{22}V \quad (12b)$$

where the coefficients j_{ik} are the elements of the Jacobian matrix \mathbf{J} evaluated at the steady state:

$$\mathbf{J} = \begin{pmatrix} 3 - 125\beta & -20 \\ 1 + 25\beta & 1 + 25\beta \\ 2\alpha & -5\alpha \\ 1 + 25\beta & 1 + 25\beta \end{pmatrix} \quad (13)$$

We seek a solution of eqn. (12) in the form of the normal modes

$$U = A e^{i(\kappa x - \omega t)}, \quad V = B e^{i(\kappa x - \omega t)} \quad (14)$$

where A and B are constants. Substitution of these forms into eqn. (12) leads to the conditions

$$(-i\omega + i\kappa\phi_P + \kappa^2 - j_{11})A - j_{12}B = 0 \quad (15a)$$

$$-j_{21}A + (-i\omega + i\kappa\phi_P + \kappa^2 - j_{22})B = 0 \quad (15b)$$

A non-trivial solution for A and B will exist only if ω satisfies the *dispersion relation*:

$$D(\kappa, \omega) \equiv \omega^2 + \{(2\kappa^2 - \text{Tr})i - 2\kappa\phi_P\}\omega - \kappa^4 - 2i\phi_P\kappa^3 + (\phi_P^2 + \text{Tr})\kappa^2 + i\phi_P \text{Tr} \kappa - \Delta = 0 \quad (16)$$

where

$$\text{Tr} = j_{11} + j_{22} \quad \text{and} \quad \Delta = j_{11}j_{22} - j_{12}j_{21} \quad (17)$$

are the trace and determinant of the Jacobian matrix \mathbf{J} .

3(a) Absolute and convective instability

A spatially distributed system is *convectively unstable* if a small perturbation induces a local growth away from the spatially uniform steady-state, but that disturbance then propagates forwards as a wave packet growing in size and with a definite ‘front’ and ‘back’. At any given location, the system experiences a finite disturbance from the spatially uniform steady state as the wave front arrives but later returns to this spatially-uniform state as the wave back passes. In contrast, we can say that the system is *absolutely unstable* in the present context if the wave packet propagates with a front but no ‘back’ (formally the wave back propagates in the opposite direction to the front) so perturbations initially increase exponentially in time at any fixed point in the laboratory frame and the system does not return to the uniform steady state after it has been disturbed.

The condition for the transition between absolute and convective instability in the present system can be determined from the dispersion relation.²¹ We begin by determining the group velocity $d\omega/d\kappa$. From eqn. (17)

$$\omega(\kappa) = \frac{1}{2}\{2\kappa\phi_P - i(2\kappa^2 - \text{Tr}) \pm \sqrt{4\Delta - \text{Tr}^2}\} \quad (18)$$

Differentiating this with respect to κ , we seek $\kappa = \kappa_0$ such that

$$\left. \frac{\partial \omega(\kappa)}{\partial \kappa} \right|_{\kappa=\kappa_0} = 0 \quad (19)$$

This gives

$$\kappa_0 = -\frac{1}{2}i\phi_P \quad (20)$$

Substitution of this result into eqn. (18) then gives

$$\omega(\kappa_0) = \frac{1}{2}\{i(\text{Tr} - \frac{1}{2}\phi_P^2) + \sqrt{4\Delta - \text{Tr}^2}\} \quad (21)$$

The condition for the transition from absolute to convective instability is given by $\text{Im}(\omega(\kappa_0)) = 0$ [so that the corresponding real part governing the time dependence of the exponent in eqn. (14) becomes zero]. If we assume the term in the discriminant in eqn. (21) is positive, then this becomes simply $\phi_P = \phi_{AC}$, where

$$\phi_{AC} = \sqrt{2\text{Tr}} \quad (22)$$

In terms of the dimensionless experimental parameters of the Lengyel–Epstein model, this becomes:

$$\phi_{AC} = \sqrt{\frac{2(3 - 5\alpha - 125\beta)}{1 + 25\beta}} \quad (23)$$

The locus of this bifurcation is shown in the ϕ_P - α parameter plane in Fig. 1: the system is absolutely unstable below this locus and convectively unstable immediately above it.

For ϕ_{AC} to be real, we require $\text{Tr}(\mathbf{J}) > 0$, which is equivalent to requiring $\alpha < \alpha_H$ as given by eqn. (11), *i.e.* the system must be below the Hopf bifurcation point (in the region of instability) of the equivalent ordinary differential equation model. The locus can be continued at small α for which the discriminant in eqn. (21) becomes negative, corresponding to $\alpha \simeq 0.07$ in Fig. 1. In this case, there are then two roots corresponding to $\text{Im}(\omega(\kappa_0)) = 0$, the lower of which is the relevant one. This section of the locus is continuous with eqn. (23), although the slope is discontinuous, and has $\phi_{AC} \rightarrow 0$ as $\alpha \rightarrow 0$.

The velocities c_+ and c_- of the front and back of the wave packet can be calculated, following Huerre,²² from the

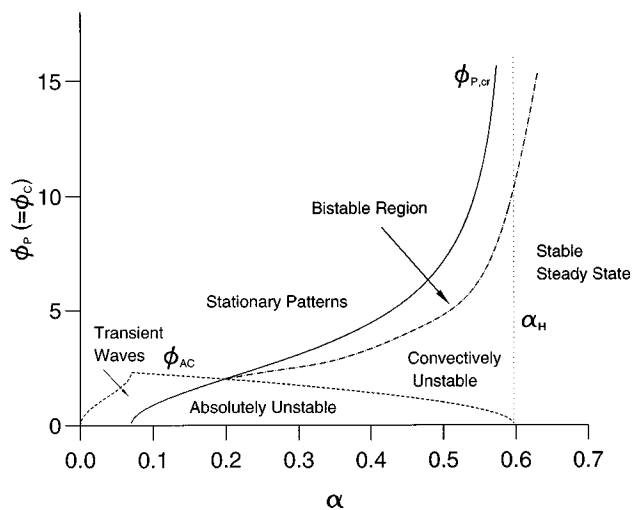


Fig. 1 Loci for different stability boundaries in the α - ϕ_p parameter plane showing regions of different responses. The region of bistability between the steady stationary patterns and the convectively unstable state, as determined by direct numerical computations, is also indicated.

Doppler effect to yield

$$c_{\pm} = \phi_p + \sqrt{2\text{Tr}} = \phi_p \pm \sqrt{\frac{2(3 - 5\alpha - 125\beta)}{1 + 25\beta}} \quad (24)$$

The lower root, c_- , is positive for the convective instability and is negative in the region of absolute instability.

3(b) Stationary patterns

The condition on the dispersion relation for a transition to a stationary pattern is $\omega = 0$ with $\text{Im}(\kappa) = 0$, so the perturbation has the form $e^{i\kappa x}$ with a purely imaginary exponent. Setting $\omega = 0$ in eqn. (17) yields

$$\kappa^4 + 2i\phi_p\kappa^3 - (\text{Tr} + \phi_p^2)\kappa^2 - i\text{Tr}\phi_p\kappa + \Delta = 0 \quad (25)$$

Setting the imaginary part equal to zero yields the condition

$$\kappa = \sqrt{\frac{1}{2}\text{Tr}(\mathbf{J})} \quad (26)$$

for the bifurcation to stationary patterns. This result can be substituted in eqn. (25) which, on rearrangement, then yields the critical flow velocity $\phi_{p,cr}$:

$$\phi_{p,cr} = \sqrt{\frac{4\Delta - \text{Tr}^2}{2\text{Tr}}} \quad (27)$$

in general terms, with

$$\phi_{p,cr} = \sqrt{\frac{100\alpha(1 + 125\beta) - (3 - 5\alpha - 125\beta)^2}{2(3 - 5\alpha - 125\beta)}} \quad (28)$$

for the present model. This locus is also shown on Fig. 1, and we expect stationary patterns to exist above the curve. We may note that $\phi_{p,cr}$ is defined only for $\alpha < \alpha_H$ ($\text{Tr} > 0$) given by eqn. (11), with $\phi_{p,cr} \rightarrow \infty$ as $\alpha \rightarrow \alpha_H$, so again this spatial structure is observable only for operating conditions for which the equivalent well-stirred batch reactor would be in its oscillatory mode.

4. Boundary conditions at $x = 0$

For reaction in a PFR of finite length, we must consider the boundary conditions. In particular, we must consider the con-

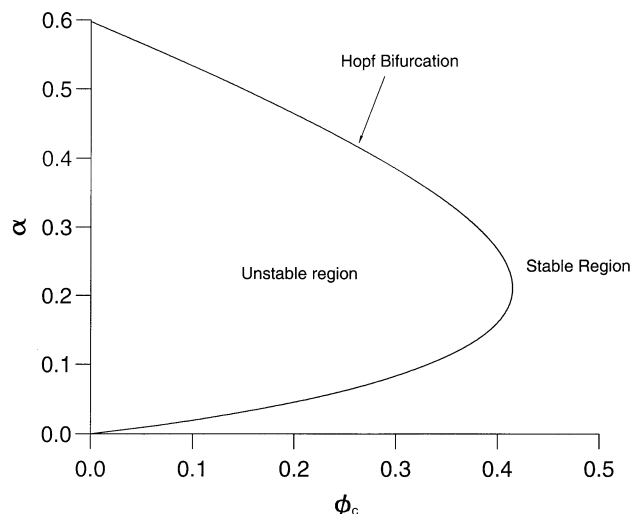


Fig. 2 Regions of stability and instability for the CSTR in the α - ϕ_c parameter plane. All computations in this paper are made of parameter values lying within the stable region so the steady-state boundary condition for the PFR is stable.

ditions imposed at the inlet to the PFR at $x = 0$ by the dynamics of the CSTR. The CSTR has a steady state satisfying $du_c/dt = dv_c/dt = 0$ in eqn. (6). The local stability of this state can be determined by standard methods. These reveal a Hopf bifurcation locus in the ϕ_c - α plane of the form shown in Fig. 2. The important feature here is that by choosing $\phi_c \gtrsim 0.414$, the steady state for the CSTR is stable for all α . We also note that for the parameter values to be used in our numerical integrations below, namely $\alpha = 0.5$ and $\alpha = 0.1$, the steady state in the CSTR is stable for $\phi_c > 0.149$ and for $\phi_c > 0.33$ respectively.

5. Numerical computations

The analysis of Section 3 has indicated the existence of at least five main regions of dynamical behaviour in the ϕ_p - α parameter plane (Fig. 1). In this section we describe the computed behaviour observed as ϕ_p is varied for two different values of α , namely for $\alpha = 0.5$ and for $\alpha = 0.1$. In each case, we take $\beta = 10^{-4}$. To reduce the number of parameters in the system, we choose here to allow the value of ϕ_c to vary so that $\phi_c = \phi_p$. (This latter condition is chosen merely for convenience, and the behaviour reported does not depend on keeping these two dimensionless groups exactly equal.) The boundary condition at $x = 0$ corresponds to the appropriate (stable) steady state for the CSTR. Note that for both these sets of results, the kinetic parameters are such that the corresponding well-stirred batch reactor would exhibit an oscillatory response.

The reaction-diffusion-advection equation (5) subject to boundary conditions (8) and (9) were solved numerically using a standard algorithm for solving the non-linear parabolic system based on the Crank-Nicolson method with Newton-Raphson iteration to solve the non-linear finite-difference equations as described in a previous paper.¹² The reactor length is set typically at $L = 100$ with a grid size of 1000 mesh points. The initial condition is taken to be the spatially uniform state, eqn. (10). The boundary condition (8) does not, in general, match this steady state and so introduces a constant 'perturbation' at $x = 0$ which is maintained for all $t > 0$.

5(a) Behaviour for $\alpha = 0.5$

With $\alpha = 0.5$, the transition from absolute to convective instability, eqn. (23), occurs at $\phi_p = \phi_{AC} = 0.99$. The response for a

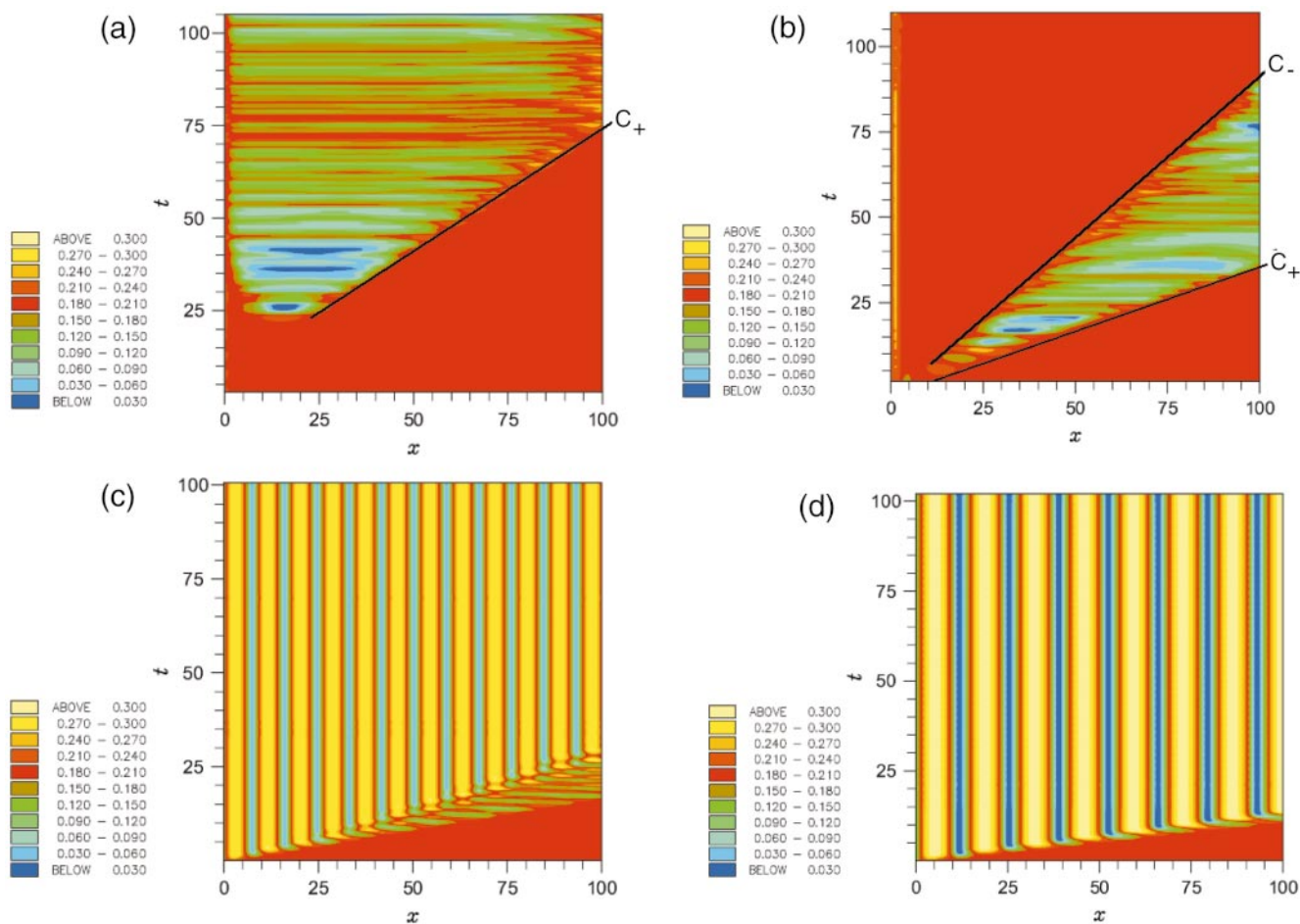


Fig. 3 Space-time plots showing the concentration u for a system with $\alpha = 0.5$ at various ϕ_p : (a) $\phi_p = 0.5 < \phi_{AC}$, corresponding to region of absolute instability; (b) $\phi_p = 2.0$, showing a convectively unstable system; (c) $\phi_p = 5.0$, lying within a convectively unstable region but showing stable stationary pattern; and (d) $\phi_p = 8.0$, showing stable stationary pattern.

system with $\phi_p = 0.5 < \phi_{AC}$ is shown as a space-time contour plot in Fig. 3(a). This response illustrates an absolute instability. The initial state of the system corresponds to the red colour. The perturbation provided by the boundary condition at $x = 0$ leads to the development of a wave that propagates as a front into the PFR. The wave can be seen to develop fully from $t \sim 25$ at a location with $x \sim 15$. The front propagates at a characteristic velocity leading to a sharp interface with a slope corresponding to the velocity. The predicted wave front velocity from eqn. (24) is $c_+ = 1.49$, agreeing well with the observed slope. Behind the wave front, the system moves away from the initial state. The system eventually appears to approach a spatially uniform oscillation about the unstable steady state as revealed by the red–yellow–green horizontal banding at long time, although a narrow boundary layer in the vicinity of the imposed (stable) boundary condition at $x = 0$ persists.

For $\phi_p = 2.0$, Fig. 3(b), the system is convectively unstable. The perturbation induces a propagating front ahead of a growing wave packet. At the rear of this wave packet, however, the system returns to the spatially uniform steady (red) state given by eqn. (10b). The different velocities of the front and rear of the wave packet are indicated by the different slopes on the space-time plot, and again agree well with the predicted values of $c_+ = 2.99$ and $c_- = 1.01$ from eqn. (24). Again, a small region of steady spatial structure at small x is now stabilised by the boundary condition imposed at $x = 0$.

The transition from convective instability to stationary patterns is predicted from eqn. (28) to occur at $\phi_p = \phi_{p,cr} = 7.15$. Space-time plots for systems with $\phi_p = 5.0 < \phi_{p,cr}$ and $\phi_p =$

$8.0 > \phi_{p,cr}$ are shown in Figs. 3(c) and (d) respectively. For the latter, a stable stationary standing-wave structure is established following the passage of the initial perturbation wave, with a characteristic wavelength $\lambda = 13.8$. Somewhat surprisingly, a stable stationary pattern, with $\lambda = 8.6$, is also observed for the system with $\phi_p = 5.0$ even though this lies in the region below the transition locus in Fig. 1.

To investigate this observation further, the evolution of the steady spatially periodic solutions emerging from the Hopf bifurcation point given by eqn. (28) was determined by integrating the steady versions of eqn. (5) backwards in x starting by making a small perturbation to the steady state (10b) and integrating until a fully periodic solution (in x) was achieved. These steady solutions were followed as a function of the parameter ϕ_p , starting close to $\phi_{p,cr}$. This reveals that, for the Lengyel–Epstein model under the present conditions, the bifurcation has a subcritical character in a similar way that it has in the well-stirred batch system. The output from the numerical integrations is combined with the computed amplitudes for the stable stationary pattern at different values of ϕ_p to produce the bifurcation diagram shown in Fig. 4. There is a turning (saddle-node) point in the stationary pattern locus at $\phi_p \approx 4.98$ at which stable and unstable branches merge. (Direct numerical integration indicates the existence of a stable pattern at $\phi_p = 4.99$ but not at 4.98.) Thus, over the range *ca.* $5.0 < \phi_p < 7.15$ there are coexisting stable and unstable stationary patterns and a convectively unstable spatially uniform state.

Further confirmation of the coexistence of the two attracting states can be obtained in the following manner. The boundary condition at $x = 0$ can be put equal to the spatially

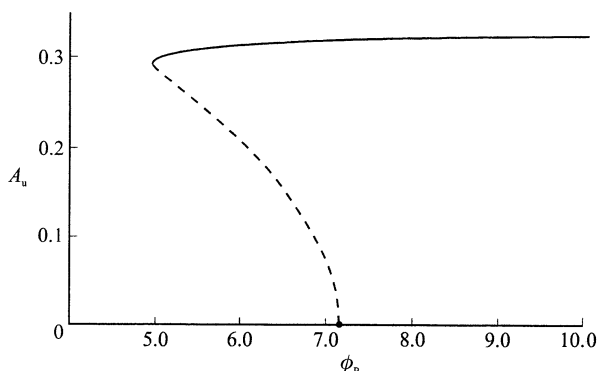


Fig. 4 Plot of amplitude of stationary pattern as a function of dimensionless flow rate ϕ_p showing subcritical nature of Hopf bifurcation at $\phi_p = \phi_{p,cr}$ with an unstable pattern emerging and growing as ϕ_p is decreased. This branch of solutions coexists with a branch of stable stationary patterns over the range *ca.* $5.0 < \phi_p < 7.15$.

uniform steady state of the PFR (u_s, v_s) onto which some perturbation δu or δv is added. By varying the magnitude of this perturbation we may seek a 'critical' case separating those conditions which are attracted to the convectively unstable state from those attracted to the coexisting stationary pattern. The long-time structure in the PFR for a system with $\phi_p = 5.0$, such that $u_s = 0.2$ and $v_s = 0.04$ and subject to an initial condition corresponding to $u(x=0) = u_s + \delta u$ and $v(x=0) = v_s$ with $\delta u = 0.09$ and 0.095 , is shown in Figs. 5(a) and (b) respectively. In the former case, the long-time structure corresponds to the convectively unstable system, with a prominent boundary structure at low x but an approach to the spatially uniform state (u_s, v_s) which has been re-established following the passage of the initial wave packet. In the latter case, the system approaches the coexisting stationary pattern. The two initial perturbations thus lie in the different basins of attrac-

tion of the two coexisting attractors. A similar feature is shown in Figs. 5(c) and (d) corresponding to slightly different initial perturbations in v , with initial conditions $u(x=0) = u_s$ and $v(x=0) = v_s + \delta v$ with $\delta v = 0.015$ and 0.020 respectively, bracketing the critical initial perturbation separating the two attracting states.

The subcritical nature of this bifurcation appears to persist over a wide region in the parameter plane, and the region of coexistence of the two attractors is indicated in Fig. 1. This response is in contrast to the supercritical nature of this bifurcation for the Brusselator model as determined by Andresen *et al.*¹⁴ The difference in the nature of this bifurcation for the two systems might have been expected from the same difference in the nature of the bifurcation to temporal oscillations in the corresponding well-stirred batch reactor models. However, we may also note that the Gray–Scott model,²³ which is closely related to the Brusselator scheme and has a supercritical Hopf bifurcation in the well-stirred case, is similar to the present model in that it shows a subcritical bifurcation between the convectively unstable and stationary pattern states in this configuration.

At large ϕ_p , the region of bistability penetrates into the region with $\alpha > \alpha_H$, indicating that for this system, flow-distributed oscillations can be obtained for parameter values beyond those for which the corresponding well-stirred batch reactor is oscillatory.

5(b) Variation of wavelength with flow velocity

The variation of the observed wavelength of the stationary pattern with the flow velocity parameter ϕ_p for a system with constant $\alpha = 0.5$ is shown in Fig. 6(a). The wavelength varies linearly with ϕ_p . The solid line superimposed on the data points is not a 'best-fit' line but is given by $\lambda = \phi_p/\omega_0$ where ω_0 is the oscillatory frequency for the corresponding well-stirred batch system with the same values of α and β . This

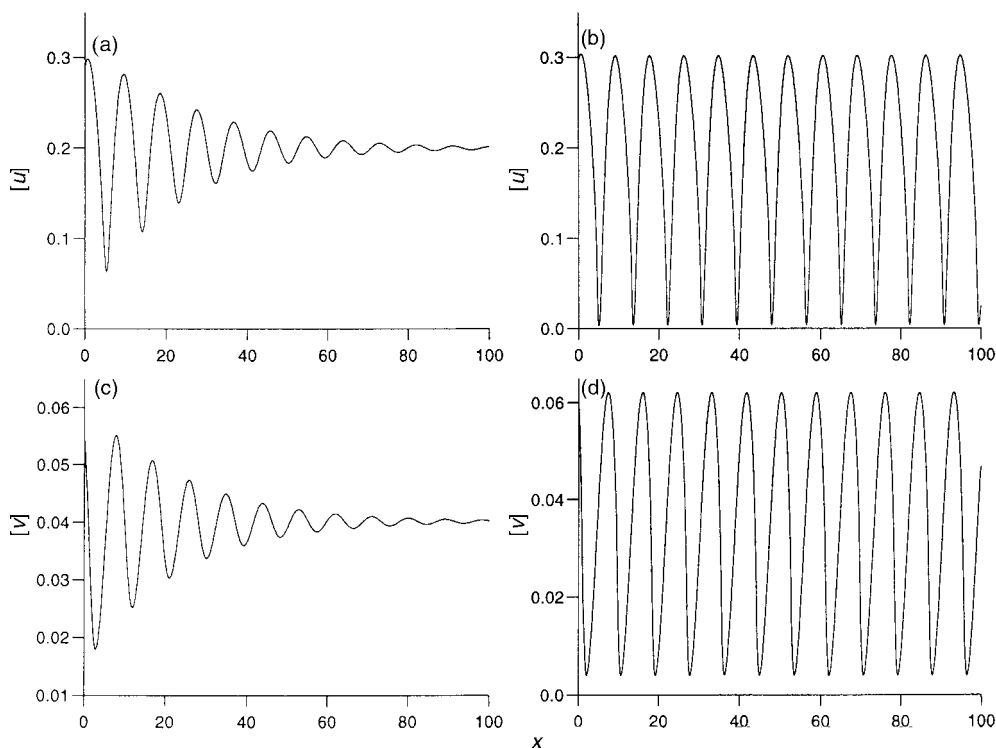


Fig. 5 Demonstration of coexistence of convectively unstable and steady stationary pattern states showing evolution from different initial conditions for a system with $\phi_p = 5.0$: (a) $u(x=0) = u_s + 0.090$ and $v = v_s$ evolving to a profile with damped spatial oscillation approaching the spatially uniform steady state; (b) same parameter values as (a) but with $u(x=0) = u_s + 0.095$ evolving to stationary pattern; (c) $v(x=0) = v_s + 0.015$ evolving to a profile with damped spatial oscillation approaching the spatially uniform steady state; and (d) same parameter values as (c) but with $v(x=0) = v_s + 0.020$ evolving to stationary pattern.

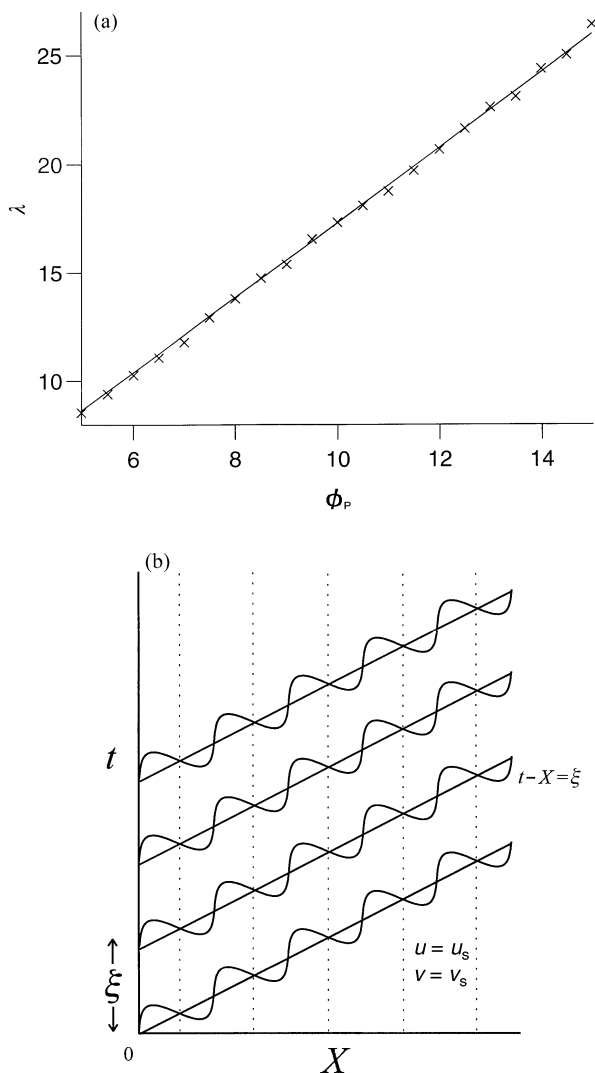


Fig. 6 (a) Variation of observed wavelength for stable stationary pattern solution with flow rate parameter ϕ_p (data points). The straight line is given by $\lambda = \phi_p/\omega_0$ where ω_0 is the oscillatory frequency of the equivalent batch system. (b) Representation of the system at large ϕ_p showing how oscillations along the characteristics lead to a stationary pattern arising in the $X-t$ frame.

reveals the essential nature of ‘flow-distributed oscillations’ as observed previously in both computation¹⁴ and experiment.¹⁵ Kuznetsov *et al.* comment¹³ on the similarity both of this relationship and of the general mechanism for stationary pattern formation for FDO with that for the emission of Vavilo–Cherenkov radiation²⁴ associated with the propagation of a charged particle in a medium of refractive index n at a velocity v exceeding the local velocity of light c/n .

The variation of pattern wavelength with flow rate is expected from eqn. (5) with ϕ_p large. Writing $x = \phi_p X$ in eqn. (5) and then letting $\phi_p \rightarrow \infty$, we obtain

$$\begin{aligned} \frac{\partial u}{\partial t} + \frac{\partial u}{\partial X} &= 1 - u - \frac{4uw}{u^2 + \beta}, \\ \frac{\partial v}{\partial t} + \frac{\partial v}{\partial X} &= \alpha \left(u - \frac{uv}{u^2 + \beta} \right) \end{aligned} \quad (29)$$

The diffusion terms, of $O(\phi_p^{-2})$ in this scaling, have been neglected. If eqn. (29) are now written in terms of the characteristic coordinate s , we obtain the ordinary differential equations

$$\frac{du}{ds} = 1 - u - \frac{4uw}{u^2 + \beta},$$

$$\frac{dv}{ds} = \alpha \left(u - \frac{uv}{u^2 + \beta} \right) \quad (30)$$

where s measures distance along a characteristic $t - X = t - \phi_p^{-1}x = \xi$, where ξ is a constant for each characteristic. Eqn. (30) are equivalent to the governing reaction rate equations for this model in a well-stirred batch reactor with the distance s replacing time t .

The ‘initial condition’ for the characteristic eqn. (30) are supplied by the ‘boundary conditions’ for the PFR at $x = 0$, *i.e.* u and v take the same constant values. Thus the dynamics along each characteristic is exactly the same, at least for each characteristic with $\xi \geq 0$. (For characteristics with $\xi < 0$, the initial conditions for eqn. (30) are the initial state of the PFR, $u = u_s$, $v = v_s$, with u and v then remaining constant at these values along the characteristics.) Hence, the initial disturbance propagates into the system along the characteristic $\xi = 0$ with a speed ϕ_p in the limit of large ϕ_p . Furthermore, if α has a value corresponding to conditions such that the batch system is oscillatory, the initial conditions produce the oscillatory response here (measured in s). As the same initial condition holds along each characteristic, the result is a steady pattern in $x-t$ space, as illustrated in Fig. 6(b). This explanation gives the result $\lambda\omega_0 = \phi_p$, shows the ‘flow distributed’ nature of these patterns and confirms that they can only arise if the kinetics are in their oscillatory model. Finally, we note that although diffusion is neglected in this analysis, it is essential in driving the instability of the uniform state to patterns.

5(c) Influence of boundary at $x = 0$

The stabilising influence of a steady state condition imposed at the inflow to the PFR at $x = 0$ on the otherwise unstable dynamics within that reactor can be illustrated numerically, by allowing a stationary pattern to develop as in the previous section, but then to change the boundary condition to match that of the uniform steady state (u_s, v_s) of the PFR.

The space-time plot for a system with $\alpha = 0.5$ and $\phi_p = 8.0$ is shown in Fig. 7. The CSTR boundary conditions are applied up to a time $t = t_1 = 40$, during which time a stationary pattern is established. At $t = t_1$, the boundary condition is adjusted to (u_s, v_s). The system responds with the collapse of the stationary pattern and approaches the uniform steady state, even though this is unstable under batch conditions. The CSTR steady state boundary conditions are re-imposed at

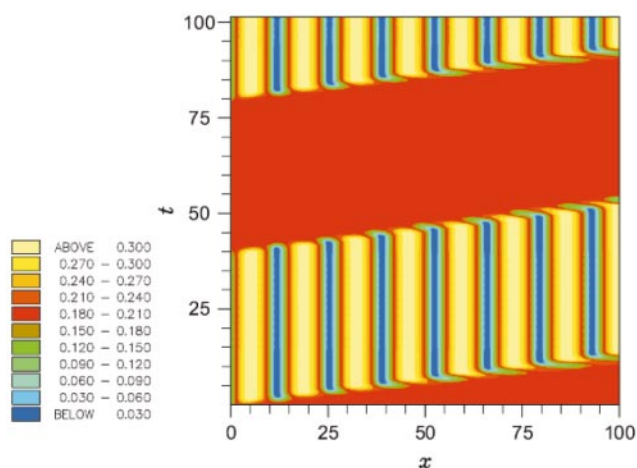


Fig. 7 Response of stationary patterns to change in boundary conditions at $x = 0$. The steady state for the CSTR is applied up to $t = 40$ and then replaced by the uniform steady-state values for $t = 40$ to $t = 80$, during which time the stationary pattern collapses. The stationary pattern is re-established when the CSTR boundary conditions are re-applied at $t = 80$.

$t = t_2 = 80$ and the stationary pattern is re-established throughout the PFR. Again the pattern develops in the wake of a front propagating from the boundary through the reactor.

5(d) Behaviour for $\alpha = 0.1$

For $\alpha = 0.1$, the loci for the absolute-to-convective instability and the onset of stationary patterns have crossed, see Fig. 1. This creates a new region lying between $\phi_p = 0.88$ and $\phi_p = 2.23$ to be investigated. Space-time plots for this case are shown in Fig. 8. For $\phi_p = 0.5$, the system lies in the region of absolute instability. The resulting space-time plot, Fig. 8(a), reveals a propagating front that takes the system from the uniform initial state to an oscillatory state. For short times after the passage of the front, there is a distribution of the phase of the oscillation along the PFR, but over time, this phase gradient disappears and the system tends towards a spatially homogeneous oscillation over almost the whole of the reactor (except for a very narrow boundary layer in the vicinity of $x = 0$).

With $\phi_p = 1.5$, the system lies above the Hopf locus for stationary patterns, but below the locus for the change from absolute to convective instability. Again, there is an initial front which takes the system from the uniform initial state, Fig. 8(b), and leaves behind an oscillatory state with distinct phase gradient along the PFR. There follows a ‘dispersion’ of this phase gradient and the system eventually tends to that of a spatially uniform oscillation at long time over the majority of the reactor. There is evidence of a narrow ‘boundary layer’ region of a stationary pattern over the range $0 < x \lesssim 8$, but the pattern does not extend beyond this into the reactor. [In

both Figs. 8(a) and (b) there is faint evidence for the propagation of a second ‘wave’ at a lower velocity than the initial front and which is associated with the change in the phase gradient.]

With $\phi_p = 2.0$, Fig. 8(c), the initial wave again sets up a temporal oscillation with a spatially distributed phase. In this case, however, there is clearly a second ‘event’ propagation behind this front and which now converts the temporal oscillation to a stationary pattern. This second ‘wave’ does not correspond to the ‘wave back’ with velocity c_- from eqn. (24) as $c_- < 0$ for these parameter values. The setting up of stationary patterns in this case is again indicative of the subcritical nature of this bifurcation: the subcritical nature seems to persist for all α . Another interesting feature of the space-time behaviour in this region before the stationary pattern is that the contour lines can develop a negative slope over some parts of the reactor, indicating that the oscillation is propagating back up the tube, in the direction of decreasing x . Such behaviour has also been reported experimentally for the BZ system.

Finally, for $\phi_p = 2.5$, which lies above the boundary for the change from absolute to convective instability, the initial front moves the system from the uniform state directly into a stationary pattern, Fig. 8(d), as before, although now with a much longer wavelength.

6. Discussion and conclusions

Chemical patterns do not require elaborate chemical complexity or unusual mass transport characteristics. ‘Flow-

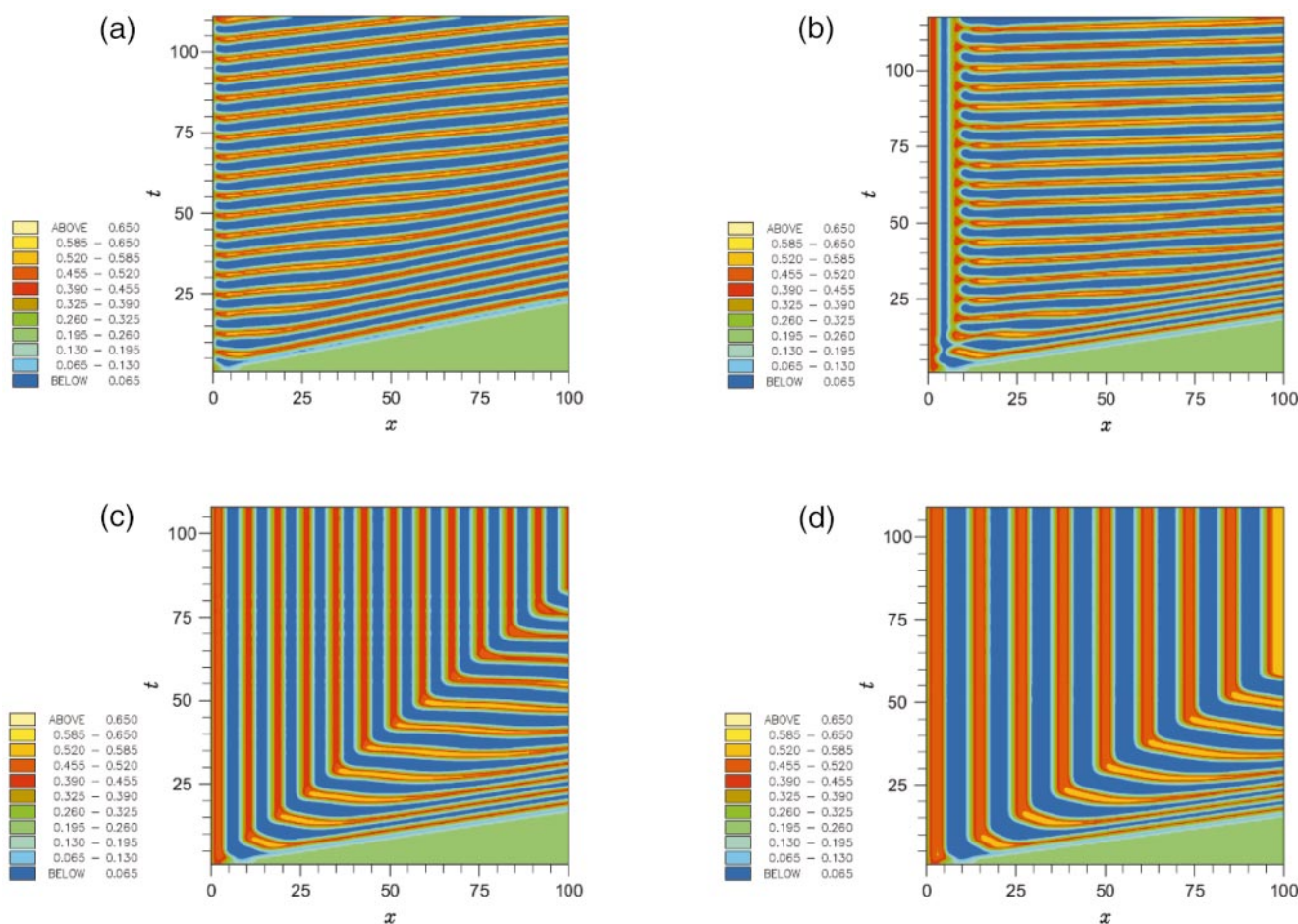


Fig. 8 Space-time plots showing the concentration u for a system with $\alpha = 0.1$ at various ϕ_p : (a) $\phi_p = 0.5 < \phi_{AC}$, corresponding to region of absolute instability; (b) $\phi_p = 1.5$, system lies above the Hopf curve but below that for the convective instability; (c) $\phi_p = 2.0$, leading to ultimate formation of a stable stationary pattern; and (d) $\phi_p = 2.5$, showing direct formation of stable stationary pattern from initial state.

distributed oscillations' arise in the simplest of open systems—the plug-flow reactor. The only requirements are that the kinetic parameters should be such that the system would support sustained oscillations in a well-stirred batch reactor and the imposition of a fixed boundary condition at the reactor inlet. There is no requirement for differential diffusion or differential flow. Above some critical flow velocity, the system will self-organise to stabilise a stationary pattern structure with the wavelength of the pattern determined by the flow velocity and the period of the autonomous chemical oscillation. Even for flow rates below this critical value, interesting spatiotemporal responses arise, with absolute or convective instabilities. (The latter is also of interest in that the system eventually approaches an essentially uniform stable steady state even though that state would be unstable in the absence of the boundary conditions. The stabilising effect of the boundary conditions is clearly demonstrated in the present work: a similar 'penetration effect' has also been reported earlier by Orteleva and Ross²⁵ in a different chemical pattern formation context.)

The results and analysis presented above indicate that absolute and convective instabilities and stationary patterns may develop for a reaction following Lengyel–Epstein kinetics. These structures should be observable in experiments as the Lengyel–Epstein model is a reasonable representation of the CDIMA reaction and the parameter values investigated here correspond to conditions accessed in other experimental studies of pattern formation.

We may also estimate the actual operating conditions under which such structures might arise. Taking a typical value $[I_2]_0 = 10^{-3} \text{ mol dm}^{-3}$, a system with $\alpha = 0.1$ and $\beta = 10^{-4}$ corresponds to $[ClO_2]_0 = 4.42 \times 10^{-3} \text{ mol dm}^{-3}$ and $[MA]_0 = 3.71 \times 10^{-3} \text{ mol dm}^{-3}$. Taking $D = 2 \times 10^{-5} \text{ cm}^2 \text{ s}^{-1}$ and values for the rate coefficients as given in Lengyel and Epstein,¹⁹ we find that the critical flow rate $\bar{\phi}_{p, cr} = 3.85 \text{ mm min}^{-1}$ and the wavelength of the stationary pattern in Fig. 8(d) would be 0.4 mm. For a system with $\alpha = 0.5$, appropriate reactant concentrations might be $[ClO_2]_0 = 8.83 \times 10^{-3} \text{ mol dm}^{-3}$ and $[MA]_0 = 7.42 \times 10^{-4} \text{ mol dm}^{-3}$, leading to $\bar{\phi}_{p, cr} = 14 \text{ mm min}^{-1}$ and a wavelength of 0.85 mm in Fig. 3(d). These are all of an order that could well be arranged in experimental reactors used in other studies.

An interesting difference between the present results and those of Kuznetsov *et al.*¹³ and of Andresen *et al.*¹⁴ is that the Hopf bifurcation to stationary patterns in the reactor is of a subcritical nature, so that patterns are found for flow rates ϕ_p below the 'critical flow rate' given by eqn. (28) and there is hysteresis between the stationary pattern and a convectively

unstable state over some range of flow rate. For the Brusselator model, this bifurcation is supercritical and so there is no hysteresis.

Acknowledgement

We thank the European Science Foundation for support under the ESF Scientific Programme *REACTOR*.

References

- 1 *Chemical Waves and Patterns*, ed. R. Kapral and K. Showalter, Kluwer, Dordrecht, 1995.
- 2 B. R. Johnson and S. K. Scott, *Chem. Soc. Rev.*, 1996, **25**, 265.
- 3 A. M. Turing, *Phil. Trans. R. Soc. Lond. B*, 1952, **237**, 37.
- 4 A. B. Rovinsky and M. Menzinger, *Phys. Rev. Lett.*, 1992, **69**, 1193.
- 5 A. B. Rovinsky and M. Menzinger, *Phys. Rev. Lett.*, 1993, **70**, 778.
- 6 Q. Ouyang, J. Boissonade, J. C. Roux and P. De Kepper, *Phys. Lett. A*, 1989, **134**, 282.
- 7 P. De Kepper, Q. Ouyang, J. Boissonade and J. C. Roux, *React. Kinet. Catal. Lett.*, 1990, **42**, 275.
- 8 Q. Ouyang, V. Castets, J. Boissonade, J. C. Roux, P. De Kepper and H. L. Swinney, *J. Chem. Phys.*, 1991, **95**, 351.
- 9 W. Y. Tam, J. A. Vastano, H. L. Swinney and W. Horsthemke, *Phys. Rev. Lett.*, 1988, **61**, 2163.
- 10 W. Y. Tam and H. L. Swinney, *Physica D*, 1990, **46**, 10.
- 11 J. A. Vastano, T. Russo and H. L. Swinney, *Physica D*, 1990, **46**, 23.
- 12 S. Kalliadasis, J. H. Merkin and S. K. Scott, *Phys. Chem. Chem. Phys.*, 2000, **2**, 2319.
- 13 S. P. Kuznetsov, E. Mosekilde, G. Dewel and P. Borckmans, *J. Chem. Phys.*, 1997, **106**, 7609.
- 14 P. Andresen, M. Bache, E. Mosekilde, G. Dewel and P. Borckmans, *Phys. Rev. E*, 1999, **60**, 297.
- 15 M. Kaern and M. Menzinger, *Phys. Rev. E*, 1999, **60**, R3471.
- 16 P. De Kepper, J. Boissonade and I. R. Epstein, *J. Phys. Chem.*, 1990, **94**, 6525.
- 17 V. Castets, E. Dulos, J. Boissonade and P. De Kepper, *Phys. Rev. Lett.*, 1990, **64**, 2953.
- 18 Q. Ouyang and H. L. Swinney, *Nature*, 1991, **352**, 610.
- 19 I. Lengyel and I. R. Epstein, *Science*, 1991, **251**, 650.
- 20 I. Lengyel and I. R. Epstein, *Chaos*, 1991, **1**, 69.
- 21 G. B. Whitham, *Linear and Nonlinear Waves*, Wiley, New York, 1973.
- 22 P. Huerre, in *Propagation in Systems Far from Equilibrium*, ed. J. E. Wesfreid, H. R. Brand, P. Manneville, G. Albinet and N. Boccara, Springer-Verlag, Berlin, 1987.
- 23 P. Gray and S. K. Scott, *Chemical Oscillations and Instabilities*, Oxford University Press, Oxford, 1990.
- 24 B. Yavorsky and A. Detlaf, *Handbook of Physics*, Mir Publishers, Moscow, 1977, p. 650.
- 25 P. J. Orteleva and J. Ross, *J. Chem. Phys.*, 1972, **56**, 287.